MITSUBISHI ELECTRIC RESEARCH LABORATORIES
http://www.merl.com

Nonlinear Model Predictive Control of Coupled Rotational-Translational Spacecraft Relative Motion

Malladi, B.; Di Cairano, S.; Weiss, A.

TR2019-064 July 11, 2019

Abstract

In this paper, a nonlinear model predictive control (NMPC) policy is developed for kinematically and dynamically coupled rotational-translational motion of a chaser spacecraft relative to an uncooperative, tumbling target asteroid. The goal of the NMPC policy is to rendezvous the chaser spacecraft, equipped with a robotic grasper, to the asteroid surface to collect a sample rock. The relative spacecraft motion model is kinematically coupled due to the non-center-of-mass points on both the target and chaser. Additionally, the chaser spacecraft is actuated by eight gimbaled thrusters, introducing dynamic coupling via control that simultaneously produces forces and torques. The combined 6-degree-of-freedom kinematically and dynamically coupled relative motion model is constrained by the NMPC policy to approach the asteroid surface via a lineof-sight cone, while enforcing thruster gimbal limit constraints. Simulations demonstrate the effectiveness of the NMPC policy in bringing the chaser spacecraft to rest relative the tumbling asteroid while satisfying state and input constraints.

American Control Conference (ACC)

Nonlinear Model Predictive Control of Coupled Rotational-Translational Spacecraft Relative Motion

Bharani P. Malladi[1], Stefano Di Cairano[2], and Avishai Weiss[2]

Abstract— **In this paper, a nonlinear model predictive control (NMPC) policy is developed for kinematically and dynamically coupled rotational-translational motion of a chaser spacecraft relative to an uncooperative, tumbling target asteroid. The goal of the NMPC policy is to rendezvous the chaser spacecraft, equipped with a robotic grasper, to the asteroid surface to collect a sample rock. The relative spacecraft motion model is kinematically coupled due to the non-center-of-mass points on both the target and chaser. Additionally, the chaser spacecraft is actuated by eight gimbaled thrusters, introducing dynamic coupling via control that simultaneously produces forces and torques. The combined 6-degree-of-freedom kinematically and dynamically coupled relative motion model is constrained by the NMPC policy to approach the asteroid surface via a line-of-sight cone, while enforcing thruster gimbal limit constraints. Simulations demonstrate the effectiveness of the NMPC policy in bringing the chaser spacecraft to rest relative the tumbling asteroid while satisfying state and input constraints.**

I. Introduction

NASA has identified rendezvous to non-cooperative free-flying space objects as a high-priority technology area [1]. In particular, rendezvous to and proximity operations near small solar system bodies such as near-Earth asteroids have been suggested priorities for future space missions [2]. Recently, the JAXA spacecraft Hayabusa2 successfully deployed two rovers to the surface of asteroid 162173 Ryugu [3]. Additionally, there has been recent interest in the mining of asteroids for raw materials by both private companies such as Planetary Resources and Deep Space Industries, and government entities such as NIAC and the USGS [4], [5].

Rendezvous to an uncooperative, tumbling asteroid target presents several challenges. The dynamics of the asteroid and a chaser spacecraft are nonlinear – both the rotational attitude dynamics with potentially large angular velocities, and the translational orbital dynamics in arbitrary orbits. Additionally, full 6 degree-of-freedom (DOF) rigid body models are necessary to describe relative rotational and translational motion between the target and chaser for rendezvous maneuvers that include important alignment between robotic graspers and surface rocks. Since graspers and rocks are generally not located at the centers of mass of their respective bodies, important kinematic coupling is established between rotation and translation [6]. Furthermore, practical real-world spacecraft thrusters aren't aligned to provide pure forces and pure torques, but rather generate forces and torques concurrently, introducing additional dynamic coupling between rotation and translation [7]. Finally, for safe and controlled approach during rendezvous that avoids collisions, the chaser spacecraft is often constrained to a line-of-sight approach cone.

Given the aforementioned challenges, the problem of 6-DOF kinematically and dynamically coupled rotational-translational spacecraft rendezvous to an uncooperative, tumbling asteroid target is an ideal candidate for model predictive control (MPC). MPC has separately been applied to point-mass-based spacecraft rendezvous and to spacecraft attitude control, see [8–12] and references therein. There has been non-MPC work on control schemes for the combined 6-DOF rigid-body rotational-translational spacecraft rendezvous problem [13], [14], and MPC-based dual quaternion spacecraft pose control [15], [16] where the authors consider position and attitude simultaneously, but their models do not exhibit any kinematic, i.e. non-center-of-mass, or dynamic, i.e. control input-based, coupling.

In this work, a nonlinear MPC (NMPC) policy is developed for kinematically and dynamically coupled rotational-translational spacecraft relative motion in order to rendezvous a chaser spacecraft, equipped with a robotic grasper, to an asteroid surface to collect a sample rock. The objective of the NMPC policy is for the chaser and its robotic grasper to track the target asteroid's orientation, angular velocity, and orbital position and velocity of the non-center-of-mass rock on the surface, that is, the objective is the stabilization of the error dynamics between the target and chaser. The relative motion model represents the chaser's relative attitude with rotation matrices in order to avoid the unwinding phenomenon [17]. The chaser spacecraft is actuated by eight gimbaled thrusters, introducing dynamic coupling via control that simultaneously produces forces and torques. The NMPC policy uses input constraints to satisfy gimbal and magnitude limits on the thrusters, and output constraints to ensure that the chaser's robotic grasper approaches the asteroid's surface rock via a line-of-sight (LOS) constraint [9], [10].

The remainder of the paper is as follows. In Section II we introduce the nonlinear 6-DOF kinematically and dynamically coupled spacecraft relative motion model. Section III gives the problem statement and describes the proposed NMPC policy. Simulation results are presented in Section IV highlighting the successful maneuver in both the asteroid frame and the inertial frame. Closing remarks are given in Section V.

[1] B. P. Malladi is with the Department of Aerospace and Mechanical Engineering, University of Arizona, Tucson, AZ 85721, USA. Email: malladi@email.arizona.edu. She was an intern at MERL during the development of this work.

[2]S. Di Cairano and A. Weiss are with Mitsubishi Research Laboratories, Cambridge, MA 02139, USA. Emails: {dicairano,weiss}@merl.com.

II. Spacecraft Model

This section begins with a summary of the notation, followed by an overview of the satellite, and details about the rotational and translational equations of motion.

A. Preliminaries and Notation

The following notation will be used throughout the paper. A frame of reference $\mathrm{F_x}$ is defined by a set of three orthonormal dextral basis vectors $\{\hat{\imath}, \hat{\jmath}, \hat{k}\}$. The vector $\vec{r}_{\mathrm{q/p}}$ denotes the position of point q relative to point p, the vector $\overset{\mathrm{x}\cdot}{\vec{r}}_{\mathrm{q/p}}$ denotes the derivative of the position of point q relative to point p with respect to frame $\mathrm{F_x}$, and the vector $\vec{\omega}_{\mathrm{y/x}}$ denotes the angular velocity of frame $\mathrm{F_y}$ relative to frame $\mathrm{F_x}$. Note that $\vec{(\cdot)}$ denotes a coordinate-free (unresolved) vector and that $(\cdot)|_x$ resolves the vector in frame $\mathrm{F_x}$. All frames are orthogonal and right-handed. $\mathbb{R}^n$ denotes the n-dimensional Euclidean space. Given a matrix $A \in \mathbb{R}^{n\times n}$, $\det(A)$ denotes its determinant, $\mathrm{tr}(A)$ denotes its trace. I_n denotes the n-dimensional identity matrix. Given a vector $x = \begin{bmatrix} x_1 & x_2 & x_3 \end{bmatrix}^\top \in \mathbb{R}^3$, $x^\times$ is the skew symmetric cross-product matrix of x given by

$$x^\times = \begin{bmatrix} 0 & -x_3 & x_2 \\ x_3 & 0 & -x_1 \\ -x_2 & x_1 & 0 \end{bmatrix}.$$

The special orthogonal group $\mathrm{SO(3)} = \{R \in \mathbb{R}^{3\times 3} : \det(R) = +1, R^\top R = I_3\}$. Principal rotations about the $\hat{\imath}$, $\hat{\jmath}$, $\hat{k}$ basis vectors by an angle α are denoted by $R_{\{\hat{\imath},\hat{\jmath},\hat{k}\}}(\alpha)$.

B. Model Overview

Consider a target and a chaser in orbit around a central body. Without loss of generality, in this work that central body is Earth. The frame $\mathrm{F_e}$ is the Earth Centered Inertial (ECI) frame, e is an unforced particle, and it is assumed that e is collocated with the center of the Earth. The target's center of mass is denoted by t and has a target-fixed frame $\mathrm{F_t}$. The target asteroid has a rock on the surface at point pt. The chaser's center of mass is denoted by c and has a chaser-fixed frame $\mathrm{F_c}$. The chaser has a robotic manipulator with an end effector at point pc. The chaser is a rectangular cuboid equipped with eight thrusters mounted on the corners of two faces of the satellite. Each thruster has a frame F_k, with an origin at point t_k for thrusters $k = 1, \ldots, 8$. The thrusters provide thrust in a line coincident with their position and the center of mass of the satellite, but are able to gimbal away from this nominal direction. The target and chaser configurations lie in the special Euclidean group $\mathrm{SE(3)} = \mathrm{SO(3)} \times \mathbb{R}^3$, that is, the set of all rotations and translations of a rigid body.

C. Rotational Dynamics

The target and chaser's attitude are given by Poisson's equation,

$$\begin{aligned} \dot{R}_{\mathrm{t/e}} &= R_{\mathrm{t/e}} {\omega^{\mathrm{t}}_{\mathrm{t/e}}}^\times, \\ \dot{R}_{\mathrm{c/e}} &= R_{\mathrm{c/e}} {\omega^{\mathrm{c}}_{\mathrm{c/e}}}^\times, \end{aligned} \tag{1}$$

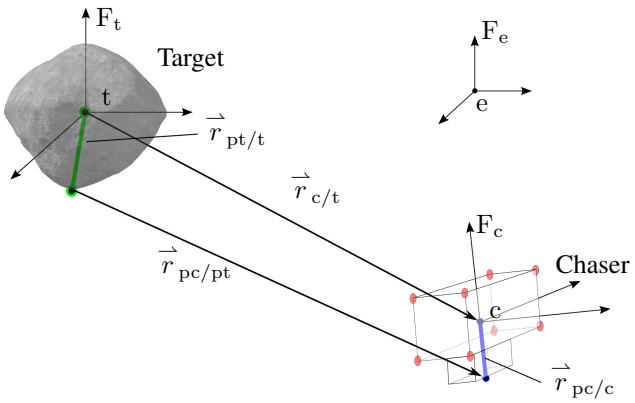

Fig. 1. Target and chaser with non-center-of-mass feature points

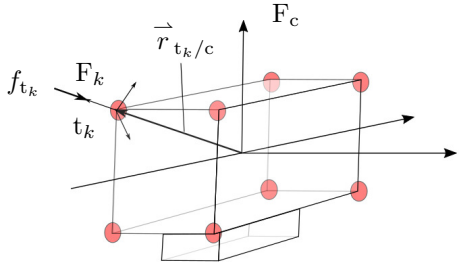

Fig. 2. Thruster configuration

where $\omega^{\{\mathrm{t,c}\}}_{\{\mathrm{t,c}\}/\mathrm{e}} \in \mathbb{R}^3$ are the angular velocities of the target and chaser frames $\mathrm{F}_{\{\mathrm{t,c}\}}$ with respect to the inertial frame $\mathrm{F_e}$ resolved in the respective target and chaser frames $\mathrm{F}_{\{\mathrm{t,c}\}}$, $\omega^\times$ is the cross-product matrix of ω, and $R_{\{\mathrm{t,c}\}/\mathrm{e}} \in \mathrm{SO(3)}$ are the rotation dyadics that transforms the inertial frame $\mathrm{F_e}$ into the target and chaser frames $\mathrm{F}_{\{\mathrm{t,c}\}}$. Therefore, $R_{\{\mathrm{t,c}\}/\mathrm{e}}$ are the proper orthogonal matrices (that is, the rotation matrices) that transform the components of vectors resolved in the target and chaser frames into the components of the same vector resolved in the inertial frame.

The dynamics of the target and chaser are given by Euler's equation

$$\begin{aligned} \dot{\omega}^{\mathrm{t}}_{\mathrm{t/e}} &= {J_{\mathrm{t}}}^{-1}(J_{\mathrm{t}}\omega^{\mathrm{t}}_{\mathrm{t/e}} \times \omega^{\mathrm{t}}_{\mathrm{t/e}} + \tau^{\mathrm{t}}_{\mathrm{p}}), \\ \dot{\omega}^{\mathrm{c}}_{\mathrm{c/e}} &= {J_{\mathrm{c}}}^{-1}(J_{\mathrm{c}}\omega^{\mathrm{c}}_{\mathrm{c/e}} \times \omega^{\mathrm{c}}_{\mathrm{c/e}} + \tau^{\mathrm{c}}_{\mathrm{p}} + \tau^{\mathrm{c}}_{\mathrm{c}}), \end{aligned} \tag{2}$$

where J_{t}, $J_{\mathrm{c}} \in \mathbb{R}^{3\times 3}$ are the moment of inertia matrices of the target and chaser respectively, $\tau^{\{\mathrm{t,c}\}}_{\mathrm{p}} \in \mathbb{R}^3$ represent the perturbation torques applied to the target and chaser, and $\tau^{\mathrm{c}}_{\mathrm{c}} \in \mathbb{R}^3$ are the control torques applied to the chaser from the thrusters, all resolved in their respective frames.

Since the objective of the chaser is to match the attitude of the target, let the relative attitude-error rotation matrix between the chaser and target be given by $R_{\mathrm{c/t}} = R^\top_{\mathrm{t/e}} R_{\mathrm{c/e}}$, which satisfies the differential equation

$$\dot{R}_{\mathrm{c/t}} = R_{\mathrm{c/t}} {\omega^{\mathrm{t}}_{\mathrm{c/t}}}^\times, \tag{3}$$

where the angular velocity error $\omega^{\mathrm{t}}_{\mathrm{c/t}}$ is defined as

$$\omega^{\mathrm{t}}_{\mathrm{c/t}} \triangleq \vec{\omega}_{\mathrm{c/t}}\Big|_t = \vec{\omega}_{\mathrm{c/e}}\Big|_t - \vec{\omega}_{\mathrm{t/e}}\Big|_t = R_{\mathrm{c/t}}\omega^{\mathrm{c}}_{\mathrm{c/e}} - \omega^{\mathrm{t}}_{\mathrm{t/e}}.$$

Taking the derivative of $\omega^{\mathrm{t}}_{\mathrm{c/t}}$ with respect to $\mathrm{F_t}$, substituting in the target and chaser dynamics $\dot{\omega}^{\mathrm{c}}_{\mathrm{c/e}}$, $\dot{\omega}^{\mathrm{t}}_{\mathrm{t/e}}$ given in

(2), and resolving into the target frame $\mathrm{F_t}$ yields,

$$\begin{aligned}\dot{\omega}^{\mathrm{t}}_{\mathrm{c/t}} &= R_{\mathrm{c/t}}\dot{\omega}^{\mathrm{c}}_{\mathrm{c/e}} - \dot{\omega}^{\mathrm{t}}_{\mathrm{t/e}} + \omega^{\mathrm{t}}_{\mathrm{c/t}} \times \omega^{\mathrm{t}}_{\mathrm{c/e}},\\ &= R_{\mathrm{c/t}}{J_{\mathrm{c}}}^{-1}(J_{\mathrm{c}}\omega^{\mathrm{c}}_{\mathrm{c/e}} \times \omega^{\mathrm{c}}_{\mathrm{c/e}} + \tau^{\mathrm{c}}_{\mathrm{p}} + \tau^{\mathrm{c}}_{\mathrm{c}})\\ &\quad -{J_{\mathrm{t}}}^{-1}(J_{\mathrm{t}}\omega^{\mathrm{t}}_{\mathrm{t/e}} \times \omega^{\mathrm{t}}_{\mathrm{t/e}} + \tau^{\mathrm{t}}_{\mathrm{p}})\\ &\quad +\omega^{\mathrm{t}}_{\mathrm{c/t}} \times (R_{\mathrm{c/t}}\omega^{\mathrm{c}}_{\mathrm{c/e}}),\end{aligned} \tag{4}$$

which, along with (3), completes the relative attitude kinematics and dynamics model.

A scalar measure of $R_{\mathrm{c/t}}$ is given by the relative eigenaxis attitude error [18]

$$\theta_{\mathrm{c/t}} = \cos^{-1}\left(\frac{1}{2}\left[\mathrm{tr}(R_{\mathrm{c/t}}) - 1\right]\right). \tag{5}$$

D. Translational Dynamics

The translational equations of motion for the target and chaser relative to the inertial frame $\mathrm{F_e}$ are given by

$$\begin{aligned}\ddot{r}^{\mathrm{e}}_{\mathrm{t/e}} &= -\mu\frac{r^{\mathrm{e}}_{\mathrm{t/e}}}{|r^{\mathrm{e}}_{\mathrm{t/e}}|^3} + \frac{f_{\mathrm{p}}}{m_{\mathrm{t}}},\\ \ddot{r}^{\mathrm{e}}_{\mathrm{c/e}} &= -\mu\frac{r^{\mathrm{e}}_{\mathrm{c/e}}}{|r^{\mathrm{e}}_{\mathrm{c/e}}|^3} + \frac{f_{\mathrm{p}}}{m_{\mathrm{c}}} + R_{\mathrm{c/e}}\frac{f_{\mathrm{c}}}{m_{\mathrm{c}}},\end{aligned} \tag{6}$$

where $r^{\mathrm{e}}_{\{\mathrm{t,c}\}/\mathrm{e}} \in \mathbb{R}^3$ are the position vectors of the target and chaser center of mass relative to the center of their central body, μ is the gravitational constant of the central body, $f_{\mathrm{p}} \in \mathbb{R}^3$ is the vector sum of orbital perturbations, $m_{\{\mathrm{t,c}\}} \in \mathbb{R}$ are the target and chaser masses, and $f_{\mathrm{c}} \in \mathbb{R}^3$ is the controllable force vector applied to the chaser in $\mathrm{F_c}$.

Consider body-fixed non-center-of-mass points pt on the target and pc on the chaser, representing a surface rock and end effector, respectively. Following [6], the relative distance between the chaser and target feature points as seen in Figure 1 is given by

$$\vec{r}_{\,\mathrm{pc/pt}} = \vec{r}_{\,\mathrm{c/t}} + \vec{r}_{\,\mathrm{pc/c}} - \vec{r}_{\,\mathrm{pt/t}}, \tag{7}$$

where $\vec{r}_{\,\mathrm{c/t}} = \vec{r}_{\,\mathrm{c/e}} - \vec{r}_{\,\mathrm{t/e}} \in \mathbb{R}^3$ is the relative distance between the center's of mass of the target and chaser rigid bodies, $\vec{r}_{\,\mathrm{pc/c}} \in \mathbb{R}^3$, $\vec{r}_{\,\mathrm{pt/t}} \in \mathbb{R}^3$, are the positions of the feature points on the chaser and target, respectively. Taking the derivative with respect to the target frame $\mathrm{F_t}$ yields

$$\overset{\mathrm{t}\cdot}{\vec{r}}_{\,\mathrm{pc/pt}} = \overset{\mathrm{t}\cdot}{\vec{r}}_{\,\mathrm{c/t}} + \overset{\mathrm{c}\cdot}{\vec{r}}_{\,\mathrm{pc/c}} + \vec{\omega}_{\mathrm{c/t}} \times \vec{r}_{\,\mathrm{pc/c}} - \overset{\mathrm{t}\cdot}{\vec{r}}_{\,\mathrm{pt/t}}. \tag{8}$$

Since the positions of the surface rock and end effector are fixed in their respective body-fixed target and chaser frames, it follows that $\overset{\mathrm{c}\cdot}{\vec{r}}_{\,\mathrm{pc/c}} = \overset{\mathrm{t}\cdot}{\vec{r}}_{\,\mathrm{pt/t}} = 0$. Taking the derivative of (8) with respect to the target frame $\mathrm{F_t}$ and resolving into $\mathrm{F_t}$ yields,

$$\begin{aligned}\ddot{\rho}^{\mathrm{t}}_{\mathrm{c/t}} \triangleq \overset{\mathrm{t}\cdot\cdot}{\vec{r}}_{\,\mathrm{pc/pt}}\Big|_t &= \ddot{r}^{\mathrm{t}}_{\mathrm{c/t}} + \dot{\omega}^{\mathrm{t}}_{\mathrm{c/t}} \times (R_{\mathrm{c/t}}r^{\mathrm{t}}_{\mathrm{pc/c}})\\ &\quad +\omega^{\mathrm{t}}_{\mathrm{c/t}} \times (\omega^{\mathrm{t}}_{\mathrm{c/t}} \times (R_{\mathrm{c/t}}r^{\mathrm{t}}_{\mathrm{pc/c}})),\end{aligned} \tag{9}$$

where $\ddot{r}^{\mathrm{t}}_{\mathrm{c/t}}$ is given by [19, Chapter 4.1, equation(4.10)]

$$\begin{aligned}\ddot{r}^{\mathrm{t}}_{\mathrm{c/t}} &= R^{\top}_{\mathrm{t/e}}(\ddot{r}^{\mathrm{e}}_{\mathrm{c/e}} - \ddot{r}^{\mathrm{e}}_{\mathrm{t/e}})\\ &\quad -2\omega^{\mathrm{t}}_{\mathrm{t/e}} \times (R^{\top}_{\mathrm{t/e}}(\dot{r}^{\mathrm{e}}_{\mathrm{c/e}} - \dot{r}^{\mathrm{e}}_{\mathrm{t/e}}))\\ &\quad -\dot{\omega}^{\mathrm{t}}_{\mathrm{t/e}} \times (R^{\top}_{\mathrm{t/e}}(r^{\mathrm{e}}_{\mathrm{c/e}} - r^{\mathrm{e}}_{\mathrm{t/e}}))\\ &\quad +\omega^{\mathrm{t}}_{\mathrm{t/e}} \times (\omega^{\mathrm{t}}_{\mathrm{t/e}} \times (R^{\top}_{\mathrm{t/e}}(r^{\mathrm{e}}_{\mathrm{c/e}} - r^{\mathrm{e}}_{\mathrm{t/e}}))).\end{aligned} \tag{10}$$

Equation (9) is the relative translational dynamics model between the chaser and target feature points pc, pt. Since the feature points are not located at the centers of mass of their respective bodies, their rotational motion about their own center of mass projected onto the translational space, kinematically couples (9) with the relative attitude kinematics (3) and dynamics (4) model via $R_{\mathrm{c/t}}$ and $\omega^{\mathrm{t}}_{\mathrm{c/t}}$.

E. Thrusters

In addition to kinematic coupling, the spacecraft relative motion model in this work exhibits dynamic coupling via the thruster configuration. Recall Figure 2. Each thruster has a position $\vec{r}_{\,\mathrm{t}_k/\mathrm{c}}$. The nominal thrust direction lies along this vector. Each thruster frame F_k has its $\hat{\jmath}$ unit vector defined such that $\hat{\jmath} = \vec{r}_{\,\mathrm{t}_k/\mathrm{c}}/|\vec{r}_{\,\mathrm{t}_k/\mathrm{c}}|$. Each force f_{t_k} is applied at the point t_k. The total force due to the thrusters applied on chaser resolved in $\mathrm{F_c}$ is given by

$$f_{\mathrm{c}} = \sum_{\mathrm{k}=1}^{8} R_{k/\mathrm{c}}f_{\mathrm{t}_k}, \tag{11}$$

where $R_{k/\mathrm{c}} \in \mathrm{SO}(3)$ is the rotation matrix that resolves the forces from thruster frame F_k to the the chaser frame $\mathrm{F_c}$. The torque produced by these thrusters relative to chaser's center of mass resolved in $\mathrm{F_c}$ is given by

$$\tau_{\mathrm{c}} = \sum_{k=1}^{8} {r_{\mathrm{t}_k}}^{\times} R_{k/\mathrm{c}}f_{\mathrm{t}_k}. \tag{12}$$

The gimbal angle of the thruster is a quantity that can be evaluated once the controller has found the control input f_{t_k}. The gimbal angles comprise two angles, α_1 and α_3, which are depicted in Fig. 3. The angles are defined such that f_{t_k} can be described by two principal rotations, yielding

$$f_{\mathrm{t}_k} = -R_{\hat{\imath}}(\alpha_1)R_{\hat{k}}(\alpha_3)\,\hat{\jmath}|_{\mathrm{F}_k}\,\|f_{\mathrm{t}_k}\|\,. \tag{13}$$

The negative sign in (13) is due to convention that the thrust is in the $-\hat{\jmath}$ direction. The controller will compute the thrust components resolved in $\mathrm{F_k}$, rather than a magnitude and two angles, because formulating the problem in terms of magnitude and angles will add sharp nonlinearities that would make the optimization more difficult.

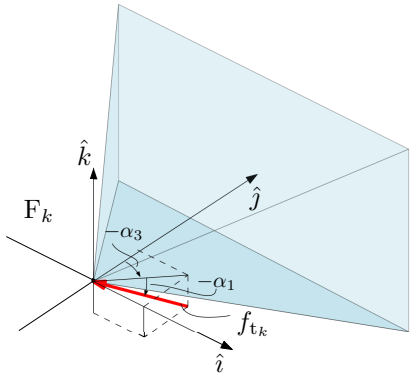

Fig. 3. Thruster configuration with gimbal angles and polyhedral pointing constraint. In this figure, the force f_{t_k} does not satisfy the positioning constraint as it is outside the blue region.

III. NMPC Policy

The main objective of this paper is to formulate a nonlinear model predictive control (NMPC) policy that simultaneously controls the translational and rotational dynamics of the chaser spacecraft feature point relative to the target feature point. Control algorithms for such maneuvers must conform to various objectives and constraints that include

1) Attitude of the chaser to track the attitude of the target
2) Relative distance between chaser and target non-center-of-mass points to be regulated
3) Non-center-of-mass point on the chaser to approach within a Line of Sight (LOS) cone from the non-center-of-mass point on the target
4) Thruster direction and magnitude limits to enforce physical limitations imposed by the propulsion system

Next we define the main components needed to formulate the NMPC policy.

A. Prediction Model

To design the control algorithm for the above mentioned spacecraft maneuver, the NMPC policy is obtained by consolidating the following model, state, input constraints.

In order to achieve offset-free steady state against modeling error or disturbances, we include integral action on the error of the non-center-of-mass feature point on the chaser with respect to the target,

$$\dot{\xi} = \rho^{\mathrm{t}}_{\mathrm{c/t}}. \tag{14}$$

Then, the prediction model for the NMPC policy is formulated as

$$\dot{x} = f(x, u) \tag{15}$$

where the state is $x = \left[R_{\mathrm{c/t}}^{\top} \; {\omega^{\mathrm{t}}_{\mathrm{c/t}}}^{\top} \; {\rho^{\mathrm{t}}_{\mathrm{c/t}}}^{\top} \; {\dot{\rho}^{\mathrm{t}}_{\mathrm{c/t}}}^{\top} \; \xi^{\top} \right]^{\top} \in \mathrm{SO}(3) \times \mathbb{R}^3 \times \mathbb{R}^3 \times \mathbb{R}^3 \times \mathbb{R}^3 = \mathcal{X}$, the input is $u = \mathrm{f_{ps}} \in \mathbb{R}^{24} = \mathcal{U}$, the vector $\mathrm{f_{ps}^{\top}} = [{f_{\mathrm{t}_1}}^{\top} \cdots {f_{\mathrm{t}_8}}^{\top}]$ contains the thrust vectors of all thrusters, and $f : \mathcal{X} \times \mathcal{U} \to \mathcal{X}$ is obtained from the attitude error kinematics equation (3), the attitude error dynamics equation (4), equation (9) describing the acceleration of the feature point, using (11), (12) to define the chaser forces and torques from the thrust vectors in $\mathrm{f_{ps}}$, and the integral action (14).

B. Constraints

The constraints enforced by the NMPC policy include thrust force constraints due to the physical limitations of the propulsion system, and line-of-sight approach constraints.

Thrust constraints are due to the propulsion system being composed of 8 thrusters located at the corners of two of the spacecraft faces where each thruster is doubly gimbaled. Then, with a slightly conservative approximation, we can satisfy the physical limitations of the propulsion system by enforcing that the forces remain in the polyhedron described by $n \in \mathbb{R}$ planes, represented by the linear constraints

$$A_k f_{\mathrm{t}_k} \leq b_k, \tag{16}$$

where $b_k \in \mathbb{R}^n$ and each of the n rows of A_k describes the normal vector of one of the n planes. In this work, $n = 4$ and is depicted in Fig. 3. The total amount of thrust that can be produced by each thruster, i.e., the thrust magnitude constraint, is a euclidean norm constraint

$$\| f_{\mathrm{t}_k} \| \leq f_{\max}. \tag{17}$$

The line-of-sight (LOS) constraint imposes that the non-center-of-mass feature point on the chaser must remain in a line of sight region of the target. This is implemented similar to the thrust constraint by enforcing $\rho^{\mathrm{t}}_{\mathrm{c/t}} \in \mathbb{R}^3$ to remain in the polyhedron described by n_{lc} hyperplanes,

$$A\rho^{\mathrm{t}}_{\mathrm{c/t}} \leq b. \tag{18}$$

For the sake of notation we compactly represent constraints (16), (17), (18), by the short notation

$$g(x, u) \leq 0, \qquad g(x, u) = \begin{bmatrix} A_{\mathrm{k}} f_{t_{\mathrm{k}}} - b_{\mathrm{k}} \\ \| f_{\mathrm{t}_k} \| - f_{\max} \\ A\rho^{\mathrm{t}}_{\mathrm{c/t}} - b \end{bmatrix}. \tag{19}$$

Constraints (16), (18), could be formulated using nonlinear functions, which avoids the need for some slightly conservative approximations we exploit here. On the other hand, as noted before, these additional nonlinearities cause the MPC problem to become significantly more complicated and hence for now we prefer the linear, slightly more conservative, formulations (16), (18).

C. Cost Function

The cost function, composed of a stage cost integrated along the prediction horizon, and of a terminal cost expressed on the state at the end of the horizon, encodes the control objectives. In this paper, the chaser objective is for the feature point to reach and stay at the target, thus attaining zero position and attitude error, with translational and angular velocities matching the target. Furthermore, in order to reduce the weight or increase the payload, the use of propellant should be minimized, which we formulate as minimizing the forces and the torques to be produced by the propulsion system. Thus, the stage cost is formulated as

$$\begin{aligned} F(x, u) := \quad & Q_{\mathrm{R}} \mathrm{tr}(D - DR^{\mathrm{t}}_{\mathrm{c/t}}) + {\omega^{\mathrm{t}}_{\mathrm{c/t}}}^{\top} Q_{\omega} \omega^{\mathrm{t}}_{\mathrm{c/t}} \\ & + {\rho^{\mathrm{t}}_{\mathrm{c/t}}}^{\top} Q_{\rho} \rho^{\mathrm{t}}_{\mathrm{c/t}} + \xi^{\top} Q_{\xi} \xi + \tau_c^{\top} W_{\tau} \tau_c \\ & + {\mathrm{f_{ps}}}^{\top} W_{\mathrm{f}} \mathrm{f_{ps}} \end{aligned} \tag{20}$$

where $Q_{\mathrm{R}} = Q_{\mathrm{R}}^{\top} > 0$, $Q_{\omega} = {Q_{\omega}}^{\top} > 0$, $Q_{\rho} = {Q_{\rho}}^{\top} > 0$, $Q_{\xi} = {Q_{\xi}}^{\top} > 0$ are matrix weights for the states, $D \in \mathbb{R}^{3\times 3}$ is a diagonal positive definite matrix, $W_{\tau} = {W_{\tau}}^{\top} > 0$, $W_{\mathrm{f}} = {W_{\mathrm{f}}}^{\top} > 0$ are matrix weights for the control inputs, and we remind that the chaser torques τ_c generated by the thrusters are function of the thrusters forces in $\mathrm{f_{ps}}$ through (12).

The terminal cost given by

$$E(x) := [{\rho^{\mathrm{t}}_{\mathrm{c/t}}}^{\top} \; {\dot{\rho}^{\mathrm{t}}_{\mathrm{c/t}}}^{\top}]^{\top} P \, [\rho^{\mathrm{t}}_{\mathrm{c/t}} \; \dot{\rho}^{\mathrm{t}}_{\mathrm{c/t}}], \tag{21}$$

where $P = P^{\top} > 0$ is a matrix weight, is mainly used here to speed up the convergence of the feature point to the target position.

D. Optimal Control Problem and NMPC Policy

The NMPC policy is based on solving in a receding horizon fashion the optimal control problem formulated based on

the dynamics (15), constraints (19), and cost function with stage cost (20) and terminal cost (21),

$$\begin{aligned} \min_{u(\cdot|t)} \quad & E(x(T|t)) + \int_0^T F(x(\tau|t),\ u(\tau|t)))\ d\tau \\ \text{s.t.} \quad & \dot{x}(\tau|t) = f(x(\tau|t), u(\tau|t)) \\ & x(0|t) = x(t) \\ & g(x(\tau|t), u(\tau|t)) \leq 0 \end{aligned} \tag{22}$$

In order to solve (22) numerically, we restrict the input to be a piecewise constant function by defining N intervals, $[t_i, t_{i+1}]$, $i \in \{0, 1, 2 \ldots, N-1\}$, $t_0 = 0$, $t_N = \tau$, $t_{i+1} - t_i = T_s = \frac{T}{N}$, and imposing $u(\tau|t) = u(t_i|t)$, for all $\tau \in [t_i, t_{i+1}]$. Then, we use collocation methods with two collocation points in each of the intervals.

As a result, the MPC policy

$$u(t) = \kappa_{\text{mpc}}(x(t)), \tag{23}$$

is obtained by computing the optimal solution $u^*(\cdot|t)$ of (22) every T_s seconds and applying $u(t+\tau) = u^*(\tau|t)$, for all $\tau \in [0, T_s)$. It shall be noted that with a proper choice of T and N, the MPC policy (23), which includes integral action due to (14), provides local stability of the closed-loop system in a region containing the goal configuration in its interior [20]. By applying specific techniques to design the terminal cost $E(x)$, possibly together with a terminal constraint $h(x(T|t) \leq 0$, one could achieve global stability in the set of states from which the optimal control problem (22) is feasible, which will also be an invariant set. We will investigate this in the future, e.g., based on the results in [12], [21], [22].

IV. Simulation Results

To demonstrate the effectiveness of the NMPC policy, consider a maneuver between the chaser and the target in circular orbits about the Earth . The target's orbital altitude is 300 km. A $1.5\text{m} \times 4\text{m} \times 1.5\text{m}$ chaser with mass $m_{\text{c}} = 4000\text{kg}$ and inertia $J_{\text{c}} = \text{diag}(6.0833, 1.5, 6.0833) \times 10^3$ kg m^2 is initially

$$r^{\text{t}}_{\text{c/t}}(0) = \begin{bmatrix} .001016052 & 116.430912621 & 0.020321028 \end{bmatrix}^\top \text{m}$$

away from the target and has initial relative velocity

$$\dot{r}^{\text{t}}_{\text{c/t}}(0) = \begin{bmatrix} 0.020321028 & 0 & -0.000117733, 1.349 \end{bmatrix}^\top \text{m/s}.$$

The non-center-of-mass feature points on the target and chaser are located at $r^{\text{t}}_{\text{pt/t}} = \begin{bmatrix} 1.1404 & 3.3462 & 5.8907 \end{bmatrix}^\top$m, and $r^{\text{c}}_{\text{pc/c}} = \begin{bmatrix} 0 & 0 & -1.75 \end{bmatrix}^\top$m. The target and chaser have initial orientations $R_{\text{t/e}}(0) = \text{diag}(1,1,1)$, $R_{\text{c/e}}(0) = \text{diag}(-1,-1,1)$ and angular velocities $\omega^{\text{t}}_{\text{t/e}}(0) = 0.0046 \times \begin{bmatrix} 1 & 1 & 1 \end{bmatrix}^\top$rad/s, $\omega^{\text{c}}_{\text{c/e}}(0) = \begin{bmatrix} 0 & 0 & 0 \end{bmatrix}^\top$rad/s. Hence, the relative distance and velocity between the non-center-of-mass feature points on target and chaser are given by

$$\begin{aligned} \rho^{\text{t}}_{\text{c/t}}(0) &= \begin{bmatrix} -1.1394 & 113.0847 & -7.6204 \end{bmatrix}^\top \text{m}, \\ \dot{\rho}^{\text{t}}_{\text{c/t}}(0) &= \begin{bmatrix} 0.0081 & 0.0039 & 1.3490 \end{bmatrix}^\top \text{m/s}. \end{aligned}$$

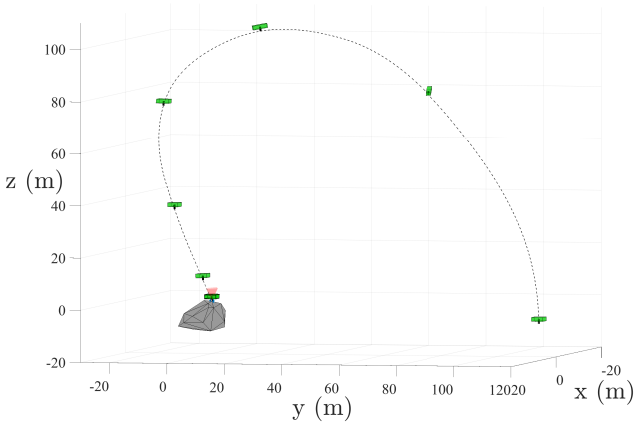

Fig. 4. Chaser and Target in target frame F_{t}. Animation available online at https://youtu.be/gj01qlexmdk

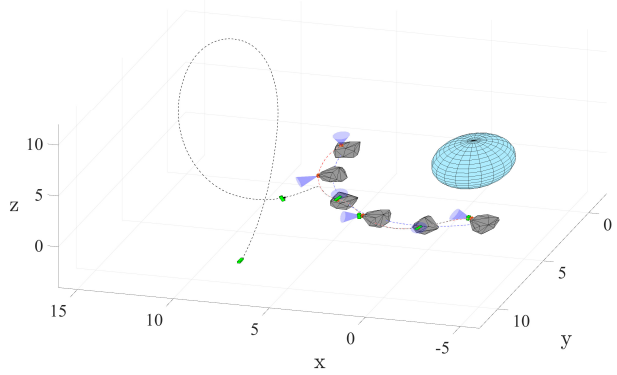

Fig. 5. Chaser and Target in Inertial frame F_{e}. Simulation results are scaled for visibility. Animation available online at https://youtu.be/92jYMyRBB0c

MPCTools [23], which provides an MPC oriented interface to CasADi [24] for Matlab, is used. CasADi in-turn utilizes IPOPT [25], a library for large-scale nonlinear optimization (see [24] for more details on CasADi). The optimal control problem (22) is solved with $N = 8$ intervals and a total time $T = 480$ s.

The LOS constraint (18) is softened via slack variables to handle initial condition infeasibility where the chaser is not aligned at $t = 0$. Since the slack variables are penalized, the NMPC policy drives the chaser feature point to the interior of the LOS polyhedron. The LOS polyhedron angle is $\pi/4$ rad. The thruster gimbal limit constraints are defined by a polyhedron with angle $\pi/4$ rad and the thrust magnitude constraint $\|f_{\text{t}_k}\| \leq f_{\text{max}}$, where $f_{\text{max}} = 20\text{N}$ The weighting matrices are $Q_R = 70$, $Q_\omega = 5I_3$, $Q_\rho = 0.01\ I_6$, $Q_\xi = 10^{-6}\ I_3$, $W_\tau = 9 \times 10^{13}\ I_3$, $W_{\text{f}} = I_{24}$.

The chaser maneuver in the target frame F_{e} is shown in Figure 4, and is available as an animation online at https://youtu.be/gj01qlexmdk. The same maneuver as seen in the inertial frame F_{e} is shown in Figure 5, and is available at https://youtu.be/92jYMyRBB0c. As seen in Figure 5, the chaser matches the angular velocity of the target as a first step before approaching the target.

The relative eigenaxis attitude and angular velocity errors between the chaser and target along with the relative position and velocity between the non-center-of-mass feature points are shown in Figure 6. Notice that for this specific maneuver,

the relative error convergence of the rotational dynamics is faster than the translational dynamics. The relative error convergence rate can be tuned as desired by altering the choice of weight matrices in the optimal control problem (22).

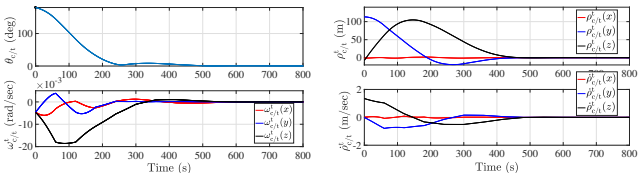

Fig. 6. Relative eigenaxis attitude error, angular velocities between chaser and target, and non-center-of-mass feature point relative distance, velocity.

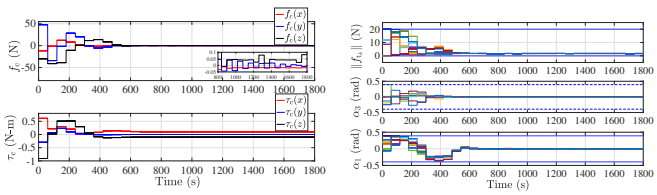

Fig. 7. Resultant forces and torques applied on the chaser, and magnitude and direction of each thruster satisfying constraints.

The resultant forces and torques acting on the center of mass of the chaser (resolved in the chaser frame) are shown in Figure 7. Since the target is tumbling, there are small non-zero forces and torques acting on the center of mass of the chaser to maintain the desired relative non-center-of-mass position and orientation at steady-state as shown in Figure 7. Integral action enables an offset-free steady-state despite the non-zero forces and torques, although in the future the stage cost (20) may be reformulated with weights on the input rate, rather than on the input magnitude. In addition, each individual thruster force f_{t_k}, $k = 1, 2, \ldots, 8$ remains in a $\pi/4$ rad polyhedron with a maximum thrust magnitude $f_{\max} = 20$ N satisfying the thruster gimbal constraints.

V. Conclusions

The main contribution of this paper was the development of a nonlinear model predictive control policy for the 6-DOF kinematically and dynamically coupled rotational-translational spacecraft relative motion model. The proposed NMPC policy is able to satisfy line-of-sight approach constraints, and thruster gimbal limit and magnitude constraints, while successfully completing the rendezvous maneuver from chaser to target, bringing relative attitude and relative feature point translational errors to zero.

For realistic implementation, some aspects still require consideration. For example, spacecraft thrusters are often "on-off" type thrusters. This quantization of thrust would change the way the thrust constraints are implemented, and change the nature of the optimization problem. Additionally, obstacle avoidance, soft-docking, and exhaust plume constraints will be addressed in future work.

References

[1] N. R. Council *et al.*, *NASA space technology roadmaps and priorities: restoring NASA's technological edge and paving the way for a new era in space*. National Academies Press, 2012.

[2] J. A. Starek, B. Açıkmeşe, I. A. Nesnas, and M. Pavone, "Spacecraft autonomy challenges for next-generation space missions," in *Advances in Control System Technology for Aerospace Applications*. Springer, 2016, pp. 1–48.

[3] JAXA Hayabusa2 Project. [Online]. Available: http://www.hayabusa2.jaxa.jp/en/

[4] L. Hall, "Robotic Asteroid Prospector (RAP) Staged from L-1: Start of the Deep Space Economy," 2013.

[5] The US Geological Survey Is Getting Serious About Space Resources and Mining. [Online]. Available: https://www.space.com/41707-space-mining-usgs-resource-survey.html

[6] S. Segal and P. Gurfil, "Effect of kinematic rotation-translation coupling on relative spacecraft translational dynamics," *Journal of Guidance, Control, and Dynamics*, vol. 32, no. 3, pp. 1045–1050, 2009.

[7] A. Walsh, S. Di Cairano, and A. Weiss, "MPC for coupled station keeping, attitude control, and momentum management of low-thrust geostationary satellites," in *American Control Conference (ACC), 2016*. IEEE, 2016, pp. 7408–7413.

[8] E. N. Hartley, "A tutorial on model predictive control for spacecraft rendezvous," in *Control Conference (ECC), 2015 European*. IEEE, 2015, pp. 1355–1361.

[9] A. Weiss, M. Baldwin, R. S. Erwin, and I. Kolmanovsky, "Model predictive control for spacecraft rendezvous and docking: Strategies for handling constraints and case studies," *IEEE Transactions on Control Systems Technology*, vol. 23, no. 4, pp. 1638–1647, 2015.

[10] H. Park, S. Di Cairano, and I. Kolmanovsky, "Model predictive control for spacecraft rendezvous and docking with a rotating/tumbling platform and for debris avoidance," in *American Control Conference (ACC), 2011*. IEEE, 2011, pp. 1922–1927.

[11] Q. Li, J. Yuan, B. Zhang, and C. Gao, "Model predictive control for autonomous rendezvous and docking with a tumbling target," *Aerospace Science and Technology*, vol. 69, pp. 700–711, 2017.

[12] U. V. Kalabić, R. Gupta, S. Di Cairano, A. M. Bloch, and I. V. Kolmanovsky, "MPC on manifolds with an application to the control of spacecraft attitude on SO(3)," *Automatica*, vol. 76, pp. 293–300, 2017.

[13] X. Li, Z. Zhu, and S. Song, "Non-cooperative autonomous rendezvous and docking using artificial potentials and sliding mode control," *Proceedings of the Institution of Mechanical Engineers, Part G: Journal of Aerospace Engineering*, p. 0954410017748988, 2018.

[14] A. Sanyal, L. Holguin, and S. P. Viswanathan, "Guidance and control for spacecraft autonomous chasing and close proximity maneuvers," *IFAC Proceedings Volumes*, vol. 45, no. 13, pp. 753–758, 2012.

[15] U. Lee and M. Mesbahi, "Constrained autonomous precision landing via dual quaternions and model predictive control," *Journal of Guidance, Control, and Dynamics*, vol. 40, no. 2, pp. 292–308, 2016.

[16] H. Dong, Q. Hu, and M. R. Akella, "Dual-quaternion-based spacecraft autonomous rendezvous and docking under six-degree-of-freedom motion constraints," *Journal of Guidance, Control, and Dynamics*, vol. 41, no. 5, pp. 1150–1162, 2017.

[17] S. P. Bhat and D. S. Bernstein, "A topological obstruction to continuous global stabilization of rotational motion and the unwinding phenomenon," *Systems & Control Letters*, vol. 39, no. 1, pp. 63–70, 2000.

[18] P. C. Hughes, *Spacecraft Attitude Dynamics*. Wiley & Sons, 1986.

[19] K. T. Alfriend, S. R. Vadali, P. Gurfil, J. P. How, and L. S. Breger, *Spacecraft Formation Flying*. Elsevier Astrodynamics Series, 2010.

[20] A. Boccia, L. Grüne, and K. Worthmann, "Stability and feasibility of state constrained MPC without stabilizing terminal constraints," *Systems & control letters*, vol. 72, pp. 14–21, 2014.

[21] J. B. Rawlings and D. Q. Mayne, "Model predictive control: Theory and design," 2009.

[22] U. Kalabić, R. Gupta, S. Di Cairano, A. Bloch, and I. Kolmanovsky, "MPC on Manifolds with an Application to SE (3)," in *American Control Conference (ACC), 2016*. IEEE, 2016, pp. 7–12.

[23] M. Risbeck and J. Rawlings, "MPCTools: Nonlinear model predictive control tools for CasADi," 2016. [Online]. Available: https://bitbucket.org/rawlings-group/mpc-tools-casadi

[24] J. A. E. Andersson, J. Gillis, G. Horn, J. B. Rawlings, and M. Diehl, "CasADi – A software framework for nonlinear optimization and optimal control," *Mathematical Programming Computation*, In Press, 2018.

[25] A. Wächter and L. T. Biegler, "On the implementation of an interior-point filter line-search algorithm for large-scale nonlinear programming," *Mathematical programming*, vol. 106, no. 1, pp. 25–57, 2006.